Remote Sensing Technology Institute

TanDEM-X Payload Ground Segment
CoSSC Generation and Interferometric Considerations
- Public -

Doc.: **TD-PGS-TN-3129**
Issue: 1.0
Date: 15.05.2012
Page: 1 of 31

DLR

TanDEM-X

Payload Ground Segment

CoSSC Generation and Interferometric Considerations

Remote Sensing Technology Institute

prepared:

_____
S. Duque   Date
ITP Developer

reviewed:

_____
U. Balss   Date
ITP Developer

reviewed:

_____
C. Rossi   Date
ITP Developer

approved:

_____
T. Fritz   Date
ITP Manager

released:

_____
W. Balzer   Date
PGS Manager

Remote Sensing Technology Institute

TanDEM-X Payload Ground Segment
CoSSC Generation and Interferometric Considerations
- Public -

Doc.: **TD-PGS-TN-3129**
Issue: 1.0
Date: 15.05.2012
Page: 2 of 31

DOCUMENT PREPARATION

The document on hand was prepared with contributions from the personnel listed below:

N. Name	Organizational Unit
Remote Sensing Technology Institute (DLR-IMF)	
U. Balss	IMF SV
H. Breit	IMF SV
S. Duque	IMF SV
T. Fritz	IMF SV
C. Rossi	IMF SV

Remote Sensing Technology Institute

TanDEM-X Payload Ground Segment
CoSSC Generation and Interferometric Considerations
- Public -

Doc.: **TD-PGS-TN-3129**
Issue: 1.0
Date: 15.05.2012
Page: 3 of 31

DOCUMENT CHANGE CONTROL

Issue	Rev.	Date	Pages	Changes	Status
1.0		15.05.2012	all	Initial issue	1.0

Remote Sensing Technology Institute

TanDEM-X Payload Ground Segment
CoSSC Generation and Interferometric Considerations
- *Public* -

Doc.: **TD-PGS-TN-3129**
Issue: 1.0
Date: 15.05.2012
Page: 4 of 31

TABLE OF CONTENTS

Remote Sensing Technology Institute

TanDEM-X Payload Ground Segment
CoSSC Generation and Interferometric Considerations
- *Public* -

Doc.: **TD-PGS-TN-3129**
Issue: 1.0
Date: 15.05.2012
Page: 5 of 31

1 DOCUMENT OVERVIEW

This document is intended to clarify **how the Coregistered Single look Slant range Complex (CoSSC) are generated** and what are the **particularities** of the monostatic active and bistatic passive coregistered images. The document is addressed to SAR experts willing to use the CoSSC products. Therefore, the basic concepts about SAR and SAR interferometry are not described. The differences between a typical monostatic TerraSAR-X (**TSX**) image and the CoSSC are stressed. The general CoSSC generation workflow is described in Section 2 and the main blocks are explained more in detail from the conceptual point of view. **The specific bistatic aspects of the CoSSC generation are remarked**. Also, **how to recover the loss of time reference of the bistatic passive image** is described in Section 3. Section 4 describes the main stages of an interferometric chain for a DEM generation using the CoSSC products. Again, the bistatic geometry particularities are emphasized on Section 4. **The different polarization working modes of the TanDEM-X mission are defined** on Section 5 and its implication on the CoSSC coregistration. Finally, in Section 6, the document describes the **novel Alternating Bistatic acquisition mode**. The coregsitration aspects of this mode and some possible applications and utilities are discussed.

2 CoSSC GENERATION

The acquired TanDEM-X (**TDX**) data from the operational modes are processed by the Integrated TanDEM Processor (**ITP**) being the CoSSCs the basic output for the experimental and also for the DEM acquisition products. Obviously, the data acquired for DEM generation are further processed by ITP up to obtain the DEM. However, the experimental products are just processed up to CoSSC generation (Fritz, 2012).

Once the acquisition data is downlinked to a receiver station, a specific ITP version carries out a screening of the data on-site. The extracted quality parameters and a small describing data package is sent online jointly with the data to the TanDEM-X Processing and Archiving Facility (PAF) in Oberpfaffenhofen (Gläser et al 2010). There, the ITP performs a quality assessment based on the data and the screening annotations named Interferometric Quality Pre-Check (IQPC) with the objective to provide a fast feedback on the success of the satellite joint acquisition. After IQPC validates the raw data able for further processing, the ITP workflow proceeds as it is illustrated in Fig. 1. The recorded raw data from the active and passive instruments are the inputs, the main processing blocks are the following:

- *Bistatic calculations and synchronization*: the small different local oscillator variations between the two instruments are calculated, thus, the corresponding timing and phase errors are corrected. The common ground coverage and the beam illumination overlap are determined. In order to proceed with the focusing of the raw data, a mutual Doppler centroid deviation analysis and the calculation of time variant bistatic geometry and focusing parameters are carried on. (Balss et al 2010, Krieger & Younis 2006)

- *SAR data focusing*: Taking into account the bistatic close formation geometry and the focusing parameters calculated on the previous step, the raw data from the two channels is focused by

Remote Sensing Technology Institute

TanDEM-X Payload Ground Segment
CoSSC Generation and Interferometric Considerations
- Public -

Doc.: **TD-PGS-TN-3129**
Issue: 1.0
Date: 15.05.2012
Page: 6 of 31

means of an enhanced version of the TerraSAR Multimode SAR Processor (TMSP) (Breit et al 2010). The output are two SSCs, a monostatic and bistatic one (Bamler et al 2007).

- *Coarse azimuth coregistration*: A **coarse azimuth coregistration** of the slave channel is carried within the azimuth focusing.

- *Spectral filtering*: The **common spectral band is filtered** in range and azimuth.

  - *Fine coregistration and resampling*: Finally, **the two SSC are fine coregistered** and the bistatic SSC is resampled to match the monostatic one (Yague-Martinez et al 2010).
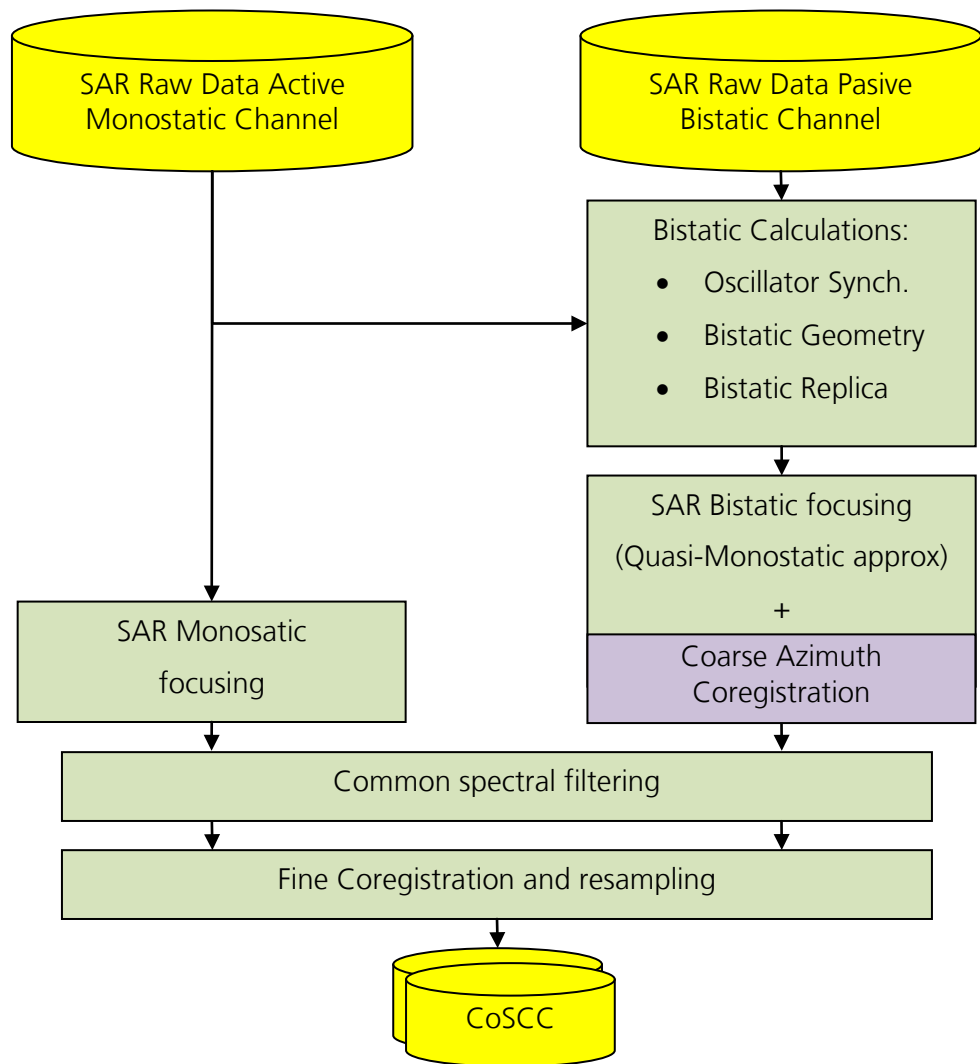
Fig. 1: CoSSC generation workflow

The main processing blocks are explained more into detail in the following subsections. The CoSSC are stored in a similar format to two TerraSAR-X level 1b products with some additional common data (Fritz 2012).

Remote Sensing Technology Institute

TanDEM-X Payload Ground Segment
CoSSC Generation and Interferometric Considerations
- *Public* -

Doc.: **TD-PGS-TN-3129**
Issue: 1.0
Date: 15.05.2012
Page: 7 of 31

2.1 SAR FOCUSING AND COARSE AZIMUTH COREGISTRATION

The quasy-monostatic TanDEM-X formation gives a range history for the bistatic acquisition that is just slightly different from the well-known monostatic hyperbola. Thus, it is licit to **approximate the true bistatic range by a hyperbola** and therefore apply a chirp scaling focusing algorithm. This valid approximation is demonstrated on (Bamler et al 2007). In order to carry out this approximation, the true range shape needs to be computed. This computation is accurately performed taking into account the range variation during the pulse transmission and reception. From Fig. 2 the range for the monostatic active and bistatic passive acquisition can be derived as

(1)
$$R_{mono}(t) = \frac{1}{2} \cdot (R_{M}(t) + R_{M}(t + \beta(t)))$$
$$R_{bist}(t) = \frac{1}{2} \cdot (R_{M}(t) + R_{S}(t + \tau(t)))$$,

where $\beta(t)$ and $\tau(t)$ are the transmission-reception delays for the monostatic and bistatic acquisition respectively while $R_{M}(t)$ and $R_{S}(t)$ refer to the range from the target to the master and slave satellite (or active and passive satellite).
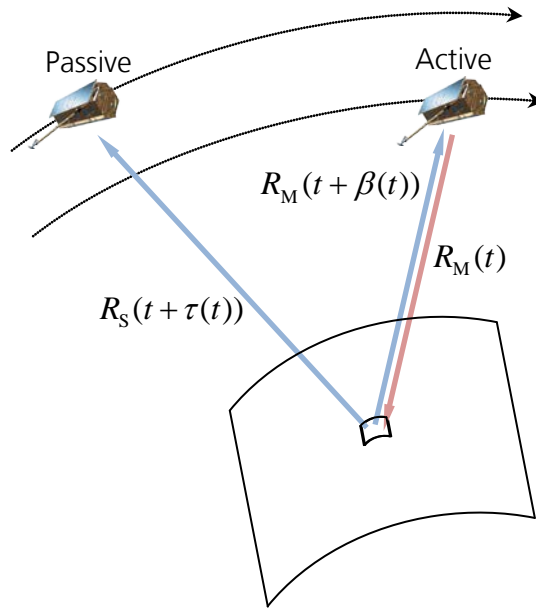

Fig. 2: TanDEM-X range sketch taking into account the time between pulse transmission and reception.

Notice that the reception delays depend on the respective range as

(2)
$$\tau(t) = \frac{2R_{bist}(t)}{c}$$
$$\beta(t) = \frac{2R_{mono}(t)}{c}$$,

which means that the monostatic and bistatic range definitions on eq. (1) are recursive. Thus, **the true bistatic range history is calculated iteratively** for a certain number of points in time and the analytical monostatic range history function

Remote Sensing Technology Institute
TanDEM-X Payload Ground Segment
CoSSC Generation and Interferometric Considerations
- *Public* -

Doc.: **TD-PGS-TN-3129**
Issue: 1.0
Date: 15.05.2012
Page: 8 of 31

(3) $\quad R_{bist}(t) \approx \tilde{R}(t) = \sqrt{\tilde{R}_0^2 + \tilde{V}_0^2 \cdot (t - \tilde{t}_0)^2}$

is fitted to them. Fig. 3 shows graphically how the analytical function (in red) is fitted to the evaluated bistatic range points (green diamonds).
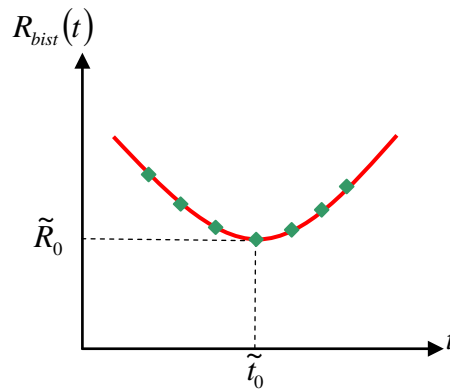

Fig. 3: Approximation of the fitted analytical function (in red) to the numerically evaluated bistatic range points (green diamonds).

This adjustment represents to find an equivalent monostatic satellite characterized by the three parameters to be found
- *The equivalent satellite velocity, $\tilde{V}_0$.*
- *The azimuth time at the apex, $\tilde{t}_0$.*
- *The range at the apex, $\tilde{R}_0$.*

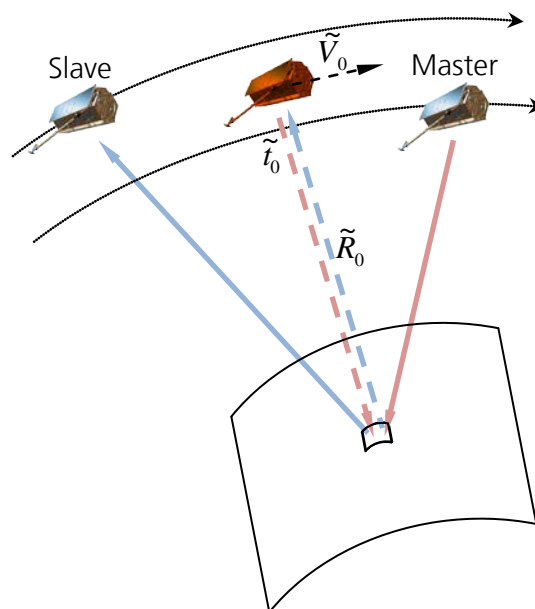The bistatic equivalent satellite is pictured on Fig. 4.

Fig. 4: Monostatic equivalent of the bistatic TanDEM-X acquisition. It is characterized by the equivalent satellite velocity, $\tilde{V}_0$, the azimuth time at the apex, $\tilde{t}_0$, and the range at the apex, $\tilde{R}_0$.

Notice that these **adjustment parameters vary for each point to be focused**. They are calculated prior to focusing at grid-points with a 300m posting covering all the scene and taking into account the

Remote Sensing Technology Institute

TanDEM-X Payload Ground Segment
CoSSC Generation and Interferometric Considerations
- Public -

Doc.: **TD-PGS-TN-3129**
Issue: 1.0
Date: 15.05.2012
Page: 9 of 31

DLR

satellite orbits and the local terrain. These obtained parameters are used to get the FM azimuth rate parameter needed for azimuth focusing as

$$(4) \qquad FM\left(R_{bist}\right) = \frac{2 \cdot \tilde{V}_0^{\,2}}{\lambda \cdot R_{bist}},$$

where λ is the wavelength. As shown on Fig. 5, **each pixel in the monostatic active and the bistatic passive image is focused in azimuth at its Zero Doppler Time (ZDT)** taking into account the antenna pattern. Notice, that for the monostatic active channel the antenna pattern refers just to the master one while for the bistatic acquisition it refers to the combined one (master + slave). The ZDT for the bistatic focusing corresponds to the $\tilde{t}_0$ found on the range history hyperbola adjustment. For sake of simplicity the ZDT for a pixel in the monostatic active acquisition will be refered as t_0 from now on. Notice that although the pixel is focused at its ZDT, the Doppler Centroid (DC) is preserved.
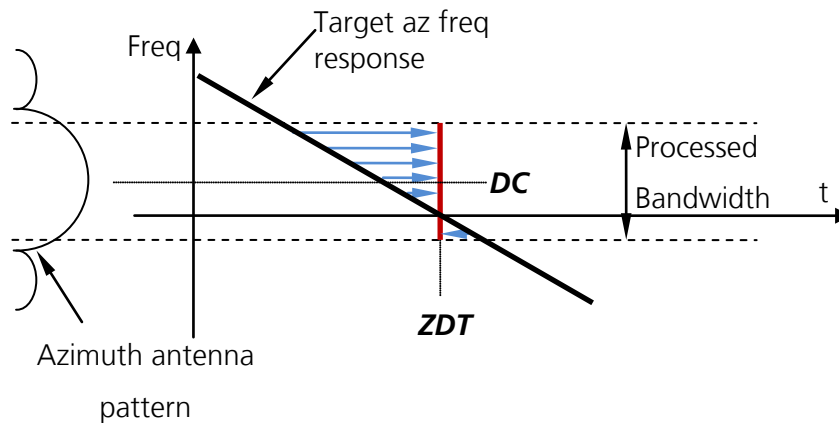

Fig. 5: Example of azimuth focusing at the target's ZDT. Each pixel in the monostatic active and the bistatic passive image is focused in azimuth at its Zero Doppler Time (ZDT) taking into account the antenna pattern and preserving its Doppler Centroid (DC).

The azimuth focusing involves also a coarse coregistration between the monostatic active and the bistatic passive channel. This coregistration is carried out for each range bin according to the ZDT differences between the monostatic active and the bistatic passive channel at the midpoint of the range bin. Therefore, the applied azimuth shift on each *ith* bin of the bistatic passive image is given by $\tilde{t}_{0,i} - t_{0,i}$, where $t_{0,i}$ is the ZDT at the midpoint of the *ith* bin of the active master image and $\tilde{t}_{0,i}$ is the bistatic ZDT related to the same area on the ground. This shift is applied at the same time of azimuth focusing by adding a phase ramp in the frequency domain. Fig. 6 illustrates the applied azimuth shift on the bistatic passive image for each range bin related to the ZDT difference.
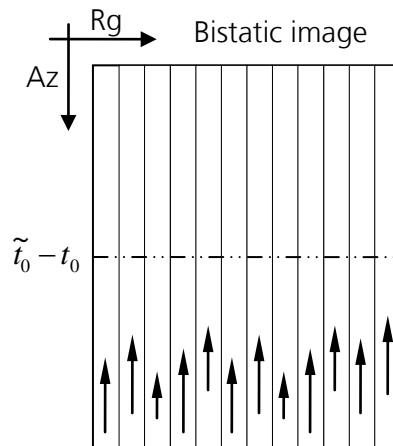
Remote Sensing Technology Institute

TanDEM-X Payload Ground Segment
CoSSC Generation and Interferometric Considerations
- Public -

Doc.: **TD-PGS-TN-3129**
Issue: 1.0
Date: 15.05.2012
Page: 10 of 31

Fig. 6: Coarse azimuth shift for each range bin according to the ZDT difference between monostatic active and bistatic passive acquisition.

2.2 COMMON SPECTRAL FILTERING

Due to the different acquisition geometries, the bistatic passive and monostatic active focused images are sampling a different part of the 2D range-azimuth spectrum. In order to improve the interferometric phase quality between the two SSCs, **the common spectrum is filtered**. This bandwidth reduction implies a loss of resolution and the impulse response of the CoSSC is widened compared to a TerraSAR-X product of same geometry and instrument and instrument settings. In practice, the geometries of the TanDEM-X close formation acquisition are not so different and **the resolution loss is not very significant (around 3-5 %)**. The resolution will be more affected when extreme baselines or Doppler centroid variations will take place.

The azimuth bandwidth shift is due mainly to the not exactly parallel orbits derived by the helix formation and the independent attitude short term variations of both satellites. These two effects are illustrated in Fig. 7, where the blue circles represent the Master and the Slave satellite while the virtual monostatic equivalent is depicted as a red circle. The respective antenna patterns are drawn in green. Notice that the monostatic equivalent position and the antenna pattern are the combination of the Master and the Slave ones. Ideally (Fig. 7a), both satellites would fly in a perfect parallel trajectories and with no antenna squint, thus the monostatic equivalent would also fly in a parallel trajectory with no squint. In this ideal scenario there would be no azimuth spectral shift between the bistatic passive and the monostatic active channel. If the two satellite's trajectories are not supposed parallel due to the TanDEM-X helix flying formation (Fig. 7b), then the equivalent monostatic and the Master satellite will have different squint angles and therefore, the azimuth spectrum will be shifted. The same effect is due to the different satellites' attitude variations (Fig. 7c). In practice, when the satellites fly in a close formation, the helix effect can be considered negligible.

Remote Sensing Technology Institute

TanDEM-X Payload Ground Segment
CoSSC Generation and Interferometric Considerations
- *Public* -

Doc.: **TD-PGS-TN-3129**
Issue: 1.0
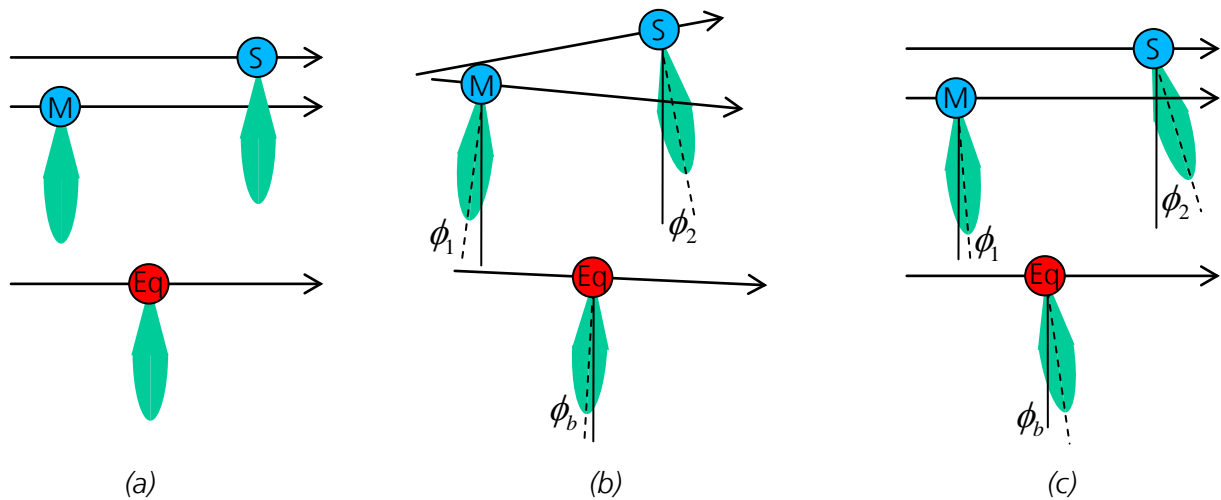Date: 15.05.2012
Page: 11 of 31

Fig. 7: Effects of azimuth frequency shift between monostatic active and bistatic passive acquisition. (a) Ideal, parallel orbits and no antenna squint, (b) Non parallel orbits and (c) Different antenna squints.

The azimuth spectral shift is derived from the estimated Doppler centroids and the azimuth processing bandwidth. **The azimuth filter is implemented block-wise** with some overlapping and it is performed range bin by range bin within each block.

The range spectral shift it is due to the slightly different acquisition geometries in the satellites' across-track direction. This shift is estimated locally by means of a simulated phase based on the satellites' orbit and the local terrain of the illuminated scene. **The range common band is also filtered locally by a block-wise filtering process**. It has to be pointed out that the adaptive filtering processes imply a variable resolution along the scene. However, if the spectral shift is small compared to the full bandwidth, **the resolution loss can be considered negligible**.

The applied spectral shift filters, in range and azimuth, are described in the given XML "***spectral_filter_frequencies.xml***". This XML is located in the "***COMMON_ANNOTATION***" directory.

2.3 FINE COREGISTRATION AND RESAMPLING

Once the images have been focused and their common spectra have been filtered, **the two images are fine coregistered** in order to have the images precisely aligned with subpixel accuracy for interferometric processing. Due to the high resolution of the system, the coregistration solution implemented in the ITP is based on local estimations of the displacement between the two images. The coregistration algorithm in the ITP is structured in the following two steps (Yague-Martinez et al 2010):

- *Geometrical Coregistration*. A geometrical calculation of the theoretical range and azimuth shifts of the two images is carried on. This calculation uses the precise orbit information from the two satellites and an external DEM.

- *Cross-Correlation*. The cross-correlation is performed with patches arranged on a grid. The information of the geometrical coregistration is used to get the patches from the bistatic passive image that maximize the overlapping with the patches on the monostatic active. The cross-correlation operation is performed using two variants, coherent and incoherent. First, a simulated topographical phase is removed in order to compensate the fringes due to the topography. Then, for a certain pair of master and slave patches, the coherent cross-correlation is calculated. In case the correlation factor is below a certain threshold the incoherent cross-

Remote Sensing Technology Institute

TanDEM-X Payload Ground Segment
CoSSC Generation and Interferometric Considerations
- Public -

Doc.: **TD-PGS-TN-3129**
Issue: 1.0
Date: 15.05.2012
Page: 12 of 31

correlation is calculated. The incoherent cross-corelation is a suboptimum estimator but it is more robust. A peak test is performed for the incoherent cross-corelation. If the peak test is not passed, then the displacement values will be just the ones determined by the geometrical coregistration.

The shift matrices for each patch in range and azimuth are obtained after the coregistration algorithm. Fig. 9 shows an example of these displacement matrices in azimuth (Fig 9a) and range (Fig 9b). Notice, that **the displacement values in the azimuth direction are around zero**, this is due to the coarse coregistration step carried out previously within the azimuth focusing.
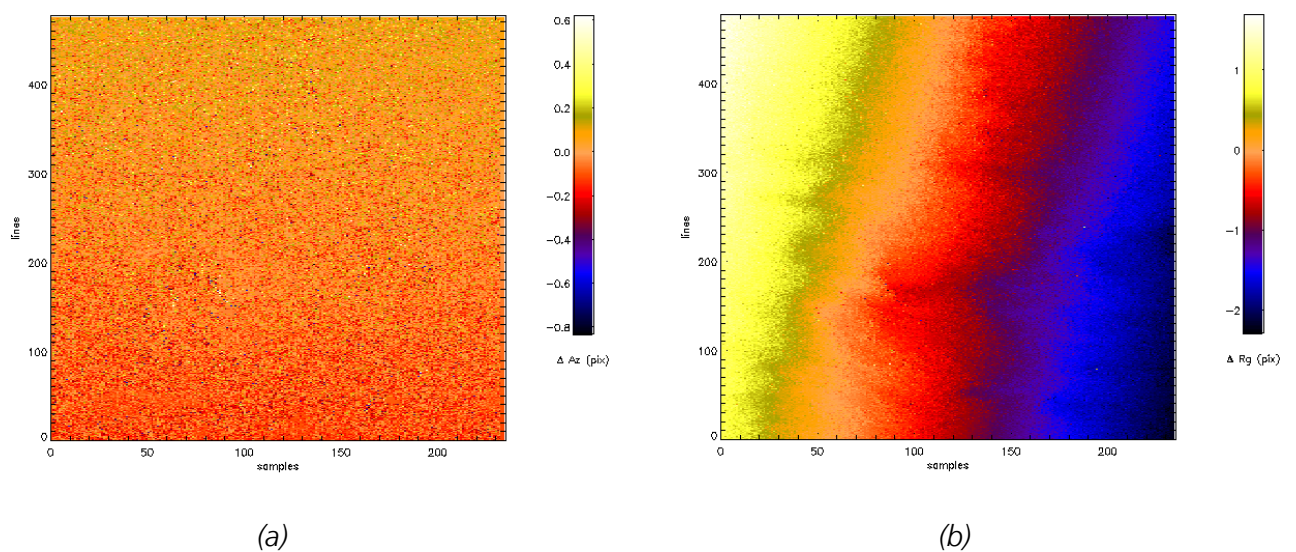

(a) *(b)*

Fig. 9: Example of displacement matrices for fine coregistration in azimuth (a) and range (b) directions.

Once these matrices are calculated, they are used to resample the bistatic passive image in order to align it to the monostatic active one with subpixel accuracy. The used displacement matrices can be found in the CoSSC delivered product at the "***COMMON_AUXRASTER***" directory under the name "***slave_shift_[az/rg].flt***".

It has to be remarked that the **bistatic passive channel has been coregistrated twice.** First a coarse coregistration within the azimuth focusing has been carried out. Second, after the spectral filtering, the bistatic passive channel has been finely coregistrated in the described procedure. Thus, it is not straightforward to relate a pixel in the bistatic passive image with the satellites' positions at its ZDT. **The time reference is lost for the bistatic passive acquisition**. This may represent a problem if one needs to simulate an interferometric phase for further processing. The necessary steps to find the satellites' positions for a specific range-azimuth pixel on the bistatic passive image are described in the next section.

Remote Sensing Technology Institute

TanDEM-X Payload Ground Segment
CoSSC Generation and Interferometric Considerations
- Public -

Doc.: **TD-PGS-TN-3129**
Issue: 1.0
Date: 15.05.2012
Page: 13 of 31

3 HOW TO FIND THE SATELLITES' FOCUSING POSITIONS ON THE BISTATIC PASSIVE IMAGE

In order to simulate the bistatic phase for further interferometric processing it is needed to know the satellites' focusing positions for each pixel on the bistatic passive image. Since the bistatic passive channel has been processed at ZDT, **to find the satellites' positions for a certain pixel is equivalent to find its ZDT**. The ZDT for a specific pixel on the bistatic passive image can be found following the next steps:

- *Locate pixel on the ground by means of the monostatic active image*. This can be done using the corresponding ZDT and the range time in the monostatic active image, the active satellite orbit and an external DEM. The monostatic ZDT can be derived from the active satellite TerraSAR-X level 1b SSC like XML file. It can be calculated using the azimuth starting time, $t_{az,start}$, located at ***<productInfo><sceneInfo><start><timeUTC>*** on the XML and adding the corresponding time to its azimuth line, j,

(5)
$$ZDT_{mono} = t_{az,start} + j \cdot t_{az,spacing} \, .$$

$t_{az,spacing}$ is the azimuth spacing time that can be found at ***<ProductInfo><imageDataInfo><imageRaster><rowSpacing>*** on the active satellite XML file. The range time can be found in the same way using the range starting time (***<ProductInfo><sceneInfo><rangeTime><firstPixel>***) and the range spacing time (***<ProductInfo><imageDataInfo><imageRaster><columnSpacing>***). The orbits are included also in the XML file under the file ***<platform><orbit>***.

Thus, it becomes a geometrical problem to retrieve the pixel's position on the ground, it will be the intersection between the isorange surface, the zero Doppler plane and the DEM. The problem can be formulated as

(6)
$$\vec{V}_{SAT,ZD} \cdot \vec{R}_{ZD} = 0$$
$$\left| \vec{R}_{ZD} \right| = t_{rg,ZD} \cdot c \quad ,$$
$$\vec{P} \in DEM$$

where $\vec{V}_{SAT,ZD}$ and $\vec{R}_{ZD}$ are the satellite's velocity and range to the point of interest at its ZDT, $t_{rg,ZD}$ is the range time, c is the wave propagation speed and $\vec{P}$ is the location of the pixel in ground range, $\vec{R}_{ZD}$ can be expressed as $\vec{R}_{ZD} = \vec{P} - \vec{P}_{SAT,ZD}$. This geometrical problem is illustrated in Fig. 10. The way to solve it has been widely studied in the literature (Curlander & McDonough 1991).
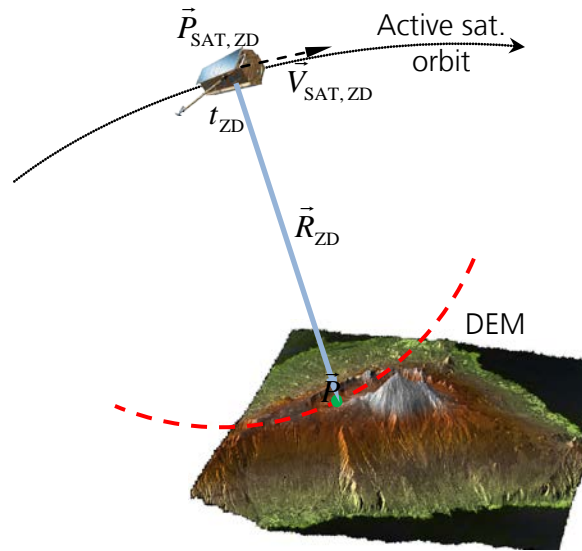
Remote Sensing Technology Institute

TanDEM-X Payload Ground Segment
CoSSC Generation and Interferometric Considerations
- Public -

Doc.: **TD-PGS-TN-3129**
Issue: 1.0
Date: 15.05.2012
Page: 14 of 31

Fig. 10: SAR monostatic pixel georeferenciation using its range and zero Doppler time, satellite's orbit and an external DEM.

- *Bistatic range calculation*. Once the pixel has been located on the ground, **the steps to find its bistatic ZDT, $\tilde{t}_0$, are the same steps carried out in the focusing to find the monostatic equivalent**. First of all, the true bistatic range history has to be calculated using the pixel position on the ground and both satelites' orbits.

- *Monostatic equivalent adjustment*. As it was performed in the processing, **the range history should be adjusted to an equivalent monostatic expression** given in (3). Therefore, the bistatic ZDT is found and the corresponding satellites' positions at that the focusing time. Thus, the synthetic bistatic phase can be retrieved.

Once these steps are carried out for all the pixels, a link between each pixel and its focusing time is established. The complete azimuth shift carried out in the CoSSC generation for each pixel will be the difference between the retrieved bistatic ZDT and the monostatic one, $\tilde{t}_0 - t_0$. Notice also that relating each pixel to its ZDT allows to find the position of the active and passive satellite at its focusing time. Thus, the calculation of the simulated phase is straightforward.

3.1 DEM ERROR SENSITIVITY TO RETRIEVE THE BISTATIC ZDT

Obviously, if the **DEM employed for the ZDT retrieval is different** from the one used in focusing, there will be some **discrepancies** between the obtained bistatic ZDT and the one used in the focusing. The DEM used for the focusing has a coarse sampling of 10 arcseconds, which implies a posting of around 300 m at the equator. Thus, the height at each sample is the average height of an area of some hectares. It has to be highlighted that in each delivered CoSSC product a downsampled version of the focusing DEM is provided. It can be found inside each SSC in the xml file **georef.xml**, which is located in the **ANNOTATION** directory. This DEM has around 500m x 500m sampling spacing, therefore, it should not present significant height variations respect the focusing DEM. A reasonable height variation of 10 meters can be assumed between both DEMs. Therefore, **the DEM provided in the georef.xml can be used for the bistatic ZDTs retrieval and for phase simulation**. Notice that

Remote Sensing Technology Institute

TanDEM-X Payload Ground Segment
CoSSC Generation and Interferometric Considerations
- *Public* -

Doc.: **TD-PGS-TN-3129**
Issue: 1.0
Date: 15.05.2012
Page: 15 of 31

since the bistatic passive channel has been coregistered, the **georef.xml** to be used should be the one related to the monostatic active channel. This section analyses the impact of using a DEM different to the one used in the focusing, as it could be the one provided in the **georef.xml** file.

The ZDT is reached in the bistatic case when the following condition is fulfilled

$$(7) \qquad \frac{V_{r,M}}{\lambda} + \frac{V_{r,S}}{\lambda} = 0 \,,$$

where $V_{r,M}$ and $V_{r,S}$ are the relative velocities to the target for the master and slave satellite respectively. The relative velocities depend on the satellites' trajectories and the range vectors to the target as

$$(8) \qquad \begin{aligned} V_{r,M} &= \vec{V}_M \cdot \hat{R}_M \\ V_{r,S} &= \vec{V}_S \cdot \hat{R}_S \end{aligned} \,,$$

being $\hat{R}_M$ and $\hat{R}_S$ the unitary range directions for the master and slave satellite. If different heights are considered, it may result in a variation of the ZDT estimation. This variation will be related to the **projection of a vector associated to a height increase on the satellites' trajectories** as

$$(9) \qquad ZDT_{dif} = h_{dif} \cdot \left(\frac{\hat{h}_{inc} \cdot \hat{V}_M}{2|\vec{V}_M|} + \frac{\hat{h}_{inc} \cdot \hat{V}_S}{2|\vec{V}_S|} \right) \,,$$

where $\hat{h}_{inc}$ is the unitary vector in the direction of the height increase. In the case of a bistatic close formation, the previous expression can be approximated by

$$(10) \qquad ZDT_{dif} \approx h_{dif} \cdot \frac{\hat{h}_{inc} \cdot \hat{V}_0}{2|\vec{V}_0|} \,,$$

taking into account the equivalent velocity vector $\vec{V}_0$. The bistatic spaceborne geometry has to take into account several factors, such as the orbit and Earth's curvature and the Earth rotation. Therefore, **the trajectory and the height increase vectors do not need to be orthogonal** as shown in Fig.11. For a reference system where the **Earth is fixed** and the orbit plane rotates, the **state vectors already contain implicitly the Earth rotation**. **Therefore, when using a reference system with fixed Earth, the earth rotation does not need to be calculated. The orbit state vectors annotated in each of the SSC products are related to an Earth fixed system.**
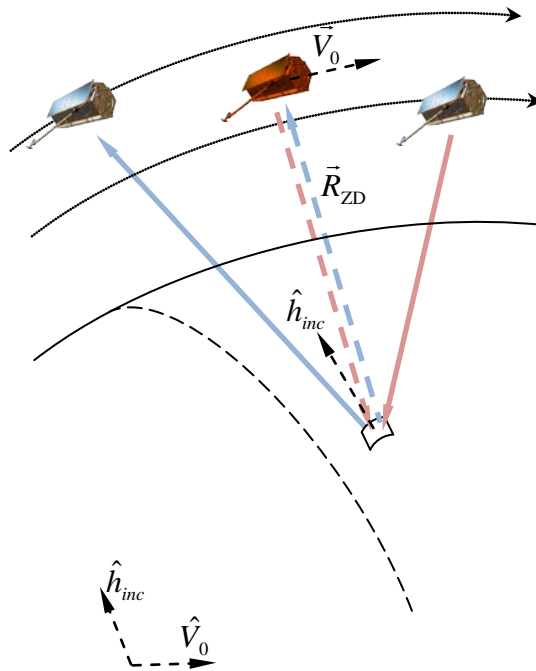
Remote Sensing Technology Institute

**TanDEM-X Payload Ground Segment
CoSSC Generation and Interferometric Considerations**
- Public -

Doc.: **TD-PGS-TN-3129**
Issue: 1.0
Date: 15.05.2012
Page: 16 of 31

Fig. 11: Illustration of $\hat{h}_{inc}$ versus $\hat{V}_0$ for a bistatic spaceborne geometry taking into account the orbit and Earth's curvature.

For a coordinate system where the **orbit plane is fixed**, the ZDT difference has to be reformulated **taking into account the earth rotation** as

(11) $ZDT_{dif} \approx h_{dif} \cdot \dfrac{\hat{h}_{inc} \cdot \left(\hat{V}_0 - \hat{V}_t\right)}{2\left|\vec{V}_0 - \vec{V}_t\right|}$,

where $\vec{V}_t$ is the velocity of the target on the ground due to the Earth rotation effect. Therefore, the ZDT difference is dependent on the target's velocity, which varies with the latitude. In order to characterize the ZDT_{dif}, a **geometric approach** taking into account an orbit of an equivalent monostatic satellite and the Earth rotation has been carried out. For this simulation the coordinate system refers to a fixed satellite's plane orbit and a rotating ellipsoid. The orbit has been simplified following the ellipsoid WGS84, taking into account the average height over the Earth, 514Km, a typical incidence angle of 39°, the orbit inclination, 97.4° deg, and the Earth has been simulated as a WGS84 rotation ellipsoid (Fig. 12).
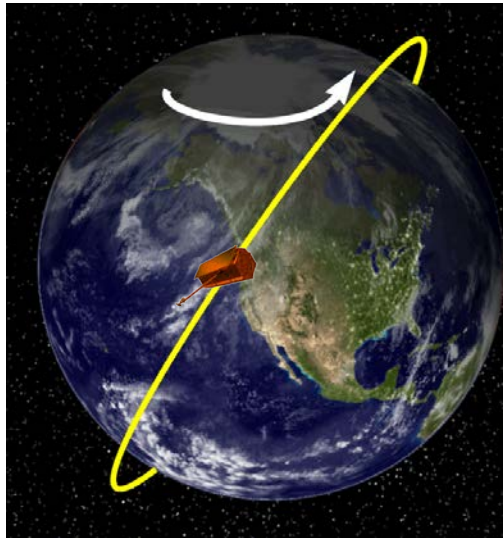
Remote Sensing Technology Institute
TanDEM-X Payload Ground Segment
CoSSC Generation and Interferometric Considerations
- Public -

Doc.: **TD-PGS-TN-3129**
Issue: 1.0
Date: 15.05.2012
Page: 17 of 31

Fig. 12: In order to characterize the ZDT_{dif}, a geometric approach taking into account an orbit of an equivalent monostatic satellite and the Earth rotation has been carried out. The orbit has been simplified following the ellipsoid WGS84, taking into account the average height over the Earth, 514Km, a typical incidence angle of 39°, the orbit inclination, 97.4° deg, and the Earth has been simulated as a WGS84 rotating ellipsoid.

The ZDT_{dif} can be related to the corresponding **displacement on the ground in the azimuth direction** due to a different height model. Fig. 13 shows the obtained displacements in the azimuth direction for targets placed at different latitudes and assuming a 10 m offset between the DEM used for focusing and the one used for the ZDT retrieval. Notice that the displacement is not zero at the equator due to the orbit's inclination. The pattern of the displacements variation is similar to a Doppler variation along the different latitudes. It has to be highlighted that for a reasonable discrepancy of 10m, the displacements in the azimuth direction are much smaller than the pixel size. Thus, **the ZDT difference can be neglected and the coarse DEM provided in the georef.xml can be used as a valid DEM to obtain the ZDTs.**
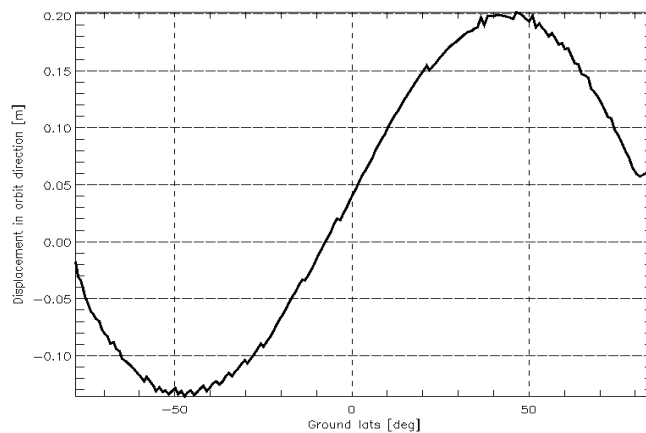

Fig. 13: Displacement in the azimuth direction due to a height discrepancy of 10m between the DEM used for focusing and the one used for the ZDT retrieval. Notice that the displacement is not zero at the equator due to the orbit's inclination.

Remote Sensing Technology Institute

TanDEM-X Payload Ground Segment
CoSSC Generation and Interferometric Considerations
- Public -

Doc.: **TD-PGS-TN-3129**
Issue: 1.0
Date: 15.05.2012
Page: 18 of 31

In order to validate the geometric approach, a simulation over a real scenario has been performed. The scene of interest is "Salar de Uyuni" located in the southwest of Bolivia at the approx. coordinates of latitude -19.85 ° and longitude -67.41°. The imaged region is composed of **a large flat salt area** and a **Tunupa's volcano**, which presents a steep topography. The height altitude over the WGS84 ellipsoid is about 3665 m for the flat salt area and 5321 m at the peak of the volcano. Fig. 14 shows the imaged area viewed by the TanDEM-X sensor. It is easy to identify the salt flat area and the volcano.
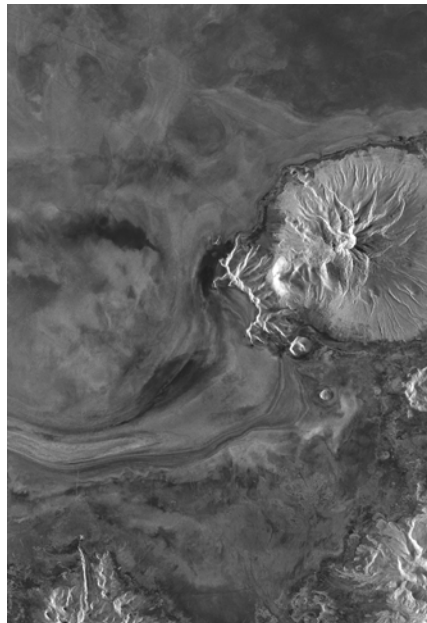

Fig. 14: Salar de Uyuni seen by TanDEM-X sensor. This region of study is composed by a large flat salt area and volcano with steep topography.

The acquisition was performed on November 16th 2010, TanDEM-X was the master satellite while TerraSAR-X was the slave. For the simulation, the DEM given in the georef.xml of the master satellite has been used as the reference DEM, as if it was the one used for focusing. The azimuth displacement of the pixels in the bistatic image due to use a different DEM for ZDT retrieval has been calculated for two cases. In the first case, **a bare WGS84 ellipsoid has been considered** as DEM to calculate the bistatic ZDTs. Notice, that **the height differences with the reference DEM for this case are large**, around 3665 in the flat salt area and up to 5321 at the volcano's peak. Secondly, the reference DEM with an offset of 10 m has been used. This last case is similar to use the provided DEM in the georef.xml than the one used in focusing, since the used in focusing is a coarse DEM with a 300m posting and the DEM given in the xml file is a downsampled version of it (around 500 m resolution).

Fig. 15a shows the displacement in the azimuth direction with respect to the reference one due to use the heights from the ellipsoid instead the reference DEM's heights. As it could be expected, the use of a height model that differs too much from the one used in focusing derives in a large ZDT discrepancies and, therefore, in a large azimuth displacement. This displacement **is totally correlated with the topography** as it is shown on Fig 15a. The flat surface shows a constant displacement around 17m, while the volcano reaches the maximum displacement of 22m at its peak. The simulated phase related to the range difference between using the ellipsoid and the reference DEM is illustrated in Fig. 15b. Not surprisingly, the simulated phase gets completely decorrelated for small height variations due the large azimuth displacement. It only shows some coherence in the flat area, where

Remote Sensing Technology Institute

TanDEM-X Payload Ground Segment
CoSSC Generation and Interferometric Considerations
- Public -

Doc.: **TD-PGS-TN-3129**
Issue: 1.0
Date: 15.05.2012
Page: 19 of 31

the fringes are a combination of the height difference at the flat surface, around 3665 m, and the azimuth displacement.

(a)   (b)
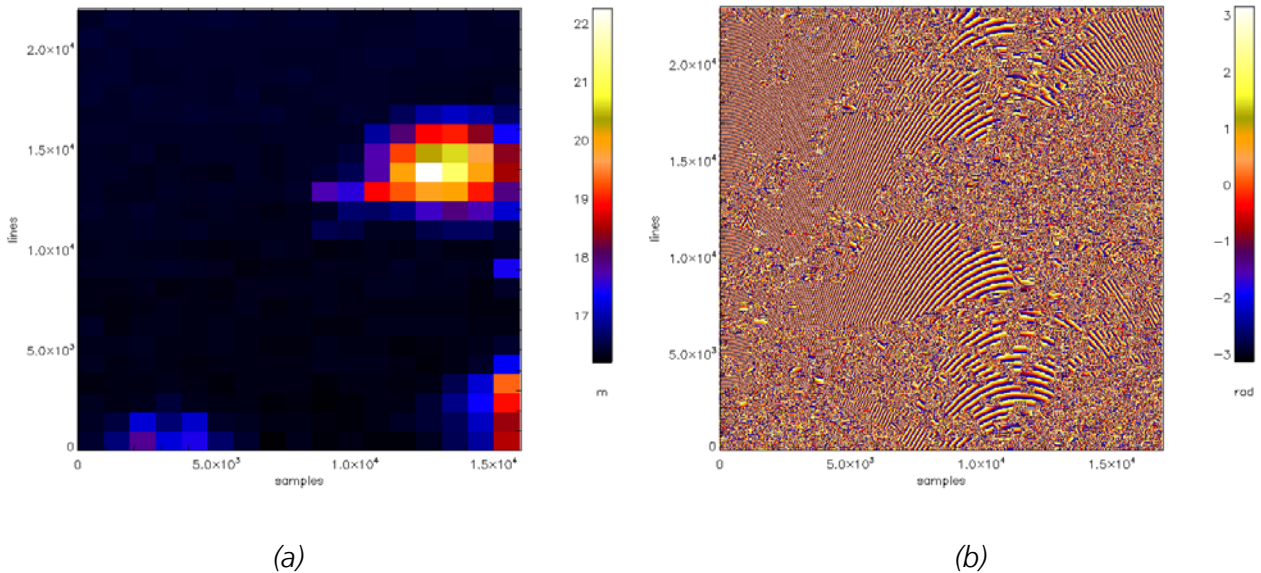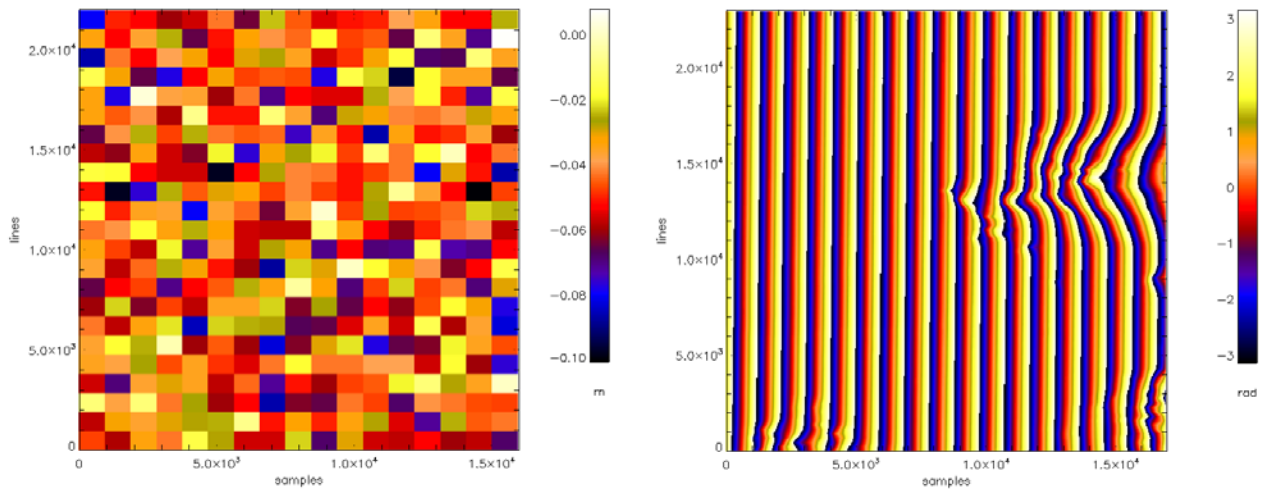
Fig. 15: (a) Displacement in the azimuth direction on the ground due to use ellipsoidal heights instead of reference DEM. This displacement is totally correlated with the topography as it can be seen on Fig 15a. The flat surface shows a constant displacement around 17m, while the volcano reaches the maximum displacement of 22m at its peak. (b) Simulated phase related to the range difference between using the reference DEM and the ellipsoid. As it could be expected, the simulated phase gets completely decorrelated for small height variations due the large azimuth displacement.

It has been demonstrated that **using the ellipsoid as a DEM to retrieve the bistatic ZDT results in large estimation errors. Thus, the ellipsoid is not a proper height model to extract the bistatic ZDTs.** However, if a DEM with a reasonable height errors of 10 m respect the DEM employed in focusing is used, the displacements in the azimuth direction are much lower. Fig. 16a shows the azimuth displacements of the area of interest for a DEM of a 10m offset respect the reference one. The errors vary from -10 cm up to 8 mm, being -4.4 cm the mean error. According to the latitude of the scene, -19.85°, the expected error from the previous geometrical approach carried on (Fig. 13) should be around -6.4 cm. Therefore, the graph on Fig. 13 gives an idea of the magnitude of the displacement errors due to use a DEM of 10m difference respect the used in focusing. In this case, the phase difference (Fig. 16b) due using a slightly different DEM is coherent for the whole scene. The fringes keep a constant fringe frequency in the flat area in the range direction related to the 10m offset. It is also possible to observe a small tilt, less than half a cycle in more than 20 thousand lines, due to the -4.4cm mean displacement in azimuth direction.

Remote Sensing Technology Institute
TanDEM-X Payload Ground Segment
CoSSC Generation and Interferometric Considerations
- Public -

Doc.: **TD-PGS-TN-3129**
Issue: 1.0
Date: 15.05.2012
Page: 20 of 31

(a)   *(b)*

Fig. 16: (a) Displacement in the azimuth direction on the ground due to use a DEM with a height offset of 10 m respect the one used in focusing. The errors are relatively small, around -4.4 cm. (b) illustrates the simulated phase related to the range difference between using the DEM with a 10m offset and the reference one. The fringes keep a constant fringe frequency in the flat area in the range direction related to the 10m offset. It is also possible to observe a small tilt, less than half a cycle in more than 20 thousand lines, due to the -4.4cm mean displacement in azimuth direction.

In any case, for all the latitudes, if a DEM that differs just 10 m from the DEM used in focusing is employed, the azimuth displacement errors do not exceed 20cm (Fig. 13). This error value is relatively small compared with the azimuth pixel dimension in the major part of cases. **The provided DEM in the GEOREF.XML is a downsampled version of the one used in the focusing. The expected discrepancy with the coarse DEM employed for focusing should not be significant. Thus, it is possible to use it for the bistatic ZDT retrieval without expecting any relevant error for the major part of applications.**

4   CONSIDERATIONS FOR DEM GENERATION BY MEANS OF A CoSSC

The CoSSC can be intereferometrically further processed by the user. This section gives some hints to take into account in the interferometric processing of the CoSSC for DEM generation. Here, it is assumed that the user is already familiarized with an interferometric chain for DEM generation. Therefore, only the main steps will be overviewed without further details. **The particularities of the bistatic geometry will be stressed**.

Fig 17. shows an example of a diagram blocks for generate a DEM from a CoSSC product. Since the CoSSC are already coregistered, the main steps for DEM generation are the following:

- *Interferogram generation*. The interferogram is generated multiplying one SSC by the conjugate of the other SSC. The interferogram can be multilooked for coherence estimation and phase noise suppression. **The resulting interferometric phase is wrapped**. There is no special bistatic remark.

Remote Sensing Technology Institute
TanDEM-X Payload Ground Segment
CoSSC Generation and Interferometric Considerations
- Public -

Doc.: **TD-PGS-TN-3129**
Issue: 1.0
Date: 15.05.2012
Page: 21 of 31

- *Phase removal.* **The interferometric phase needs to be unwrapped** to recover the absolute phase value. The phase unwrapping is the most difficult stage in an interferometric chain. As a consequence, it is recommendable to remove the a priori known phase from the interferogram. In this way, the residual phase will be smoother and, therefore, easier to unwrap**. The phase to be removed should be calculated geometrically using the two satellites orbits, the previously calculated ZDTs and an external DEM**, it may be the one provided in the GEOREF.XML, **or an ellipsoid model (flat-earth phase).**

- *Phase unwrapping*. The objective of phase unwrapping is to obtain an absolute phase from the wrapped interferogram phase. **The bistatic geometry is not involved in this step**. Thus, any of the already existent phase unwrapped algorithms can be applied. The phase unwrapping is one of the most difficult processes in an interferometric chain. This problem has been widely studied and there are many proposed solutions on the literature. Some of the most popular algorithms for phase unwrapping are based on the **Minimum Cost Flow** (**MCF**) like (Constantini 1998).

- *Absolute phase calibration*. Once the phase has been unwrapped, **there is still an absolute phase offset due to the unknown number of cycles that needs to be restored**. The most common used method to retrieve this phase offset is the use of **Ground Control Points** (**GPC**). The GPC are identified on the images that form the interferogram and the **theoretical simulated bistatic phase is calculated taking into account the bistatic geometry and the corresponding ZDTs in the two images**. Usually, more than one control point is used in order to minimize positioning errors. Other methods to obtain the phase offset are based on a **phase reference** that can be calculated by means of a **simulated bistatic phase** using a DEM or a radargrametric approach (Rossi et al 2012).

- *Geocoding*. **The geocoding process has to take into account the bistatic geometry**. The classical equation system to geocode each pixel composed by the Doppler, range and bistatic interferometric equations has to be reformulated as

$$\vec{V}_M\left(t_{az,M}\right)\cdot\left(\vec{P}_M\left(t_{az,M}\right)-\vec{P}\right)=0$$

(12) $$\left\|\vec{P}_M\left(t_{az,M}\right)-\vec{P}\right\|=t_{rg,M}\cdot c$$.

$$\left\|\vec{P}_M\left(t_{az,M}\right)-\vec{P}\right\|-\left\|\vec{P}_S\left(t_{az,S}\right)-\vec{P}\right\|=-\frac{\lambda}{2\pi}\left(\psi_{unw}+\psi_{off}\right)$$

Where $\vec{P}_M\left(t_{az,M}\right)$ and $\vec{P}_S\left(t_{az,S}\right)$ are the master and slave satellites' positions at the respective master and slave azimuth focusing times, $t_{az,M}$ and $t_{az,S}$, $\vec{P}$ is the unknown target position, $t_{rg,M}$ the master range time, c is the wave propagation velocity, $\vec{V}_M\left(t_{az,M}\right)$ is the master velocity vector at the master focusing time and ψ_{unw} and ψ_{off} are the unwrapped and the offset phase. **For an accurate geocoding the atmospheric delay should be taken into account**. It can be divided in two parts, the ionospheric and tropospheric delay. The ionospheric path delay is variable and depends on the Total Electron Content (TEC) as (Breit et al 2010, Rossi et al 2010).

(13) $$\Delta R_{iono}\left(\theta_{inc}\right)\approx\frac{K\cdot TEC}{f^2\cdot\cos(\theta_{inc})} .$$

The **square frequency dependency, f^2, makes this delay very small for an X-band system**, about 2cm for an average TEC of 5 TECU. However, **the tropospheric delay has a**

greater impact on X-band. The simple approach used in TMSP models the tropospheric delay is

(14) $$\Delta R_{tropo}\left(h,\theta_{inc}\right) \approx \frac{ZPD}{\cos(\theta_{inc})} \cdot e^{\left(-\frac{h}{H}\right)}.$$

The Zenith Path Delay is fixed to a constant 2.3m, the reference height H is set to 6000m and h is the scene average height, which can be extracted from a coarse DEM. For an incidence angle of 40° and an average height of 1000m ($\theta_{inc} = 40^0, h = 1000m$), the delay is 2.5m. **These atmospheric delays should be taking into account in the range master equation in (12) compensating properly the range time, $t_{rg,M}$**. Also, for a more accurate geocoding, due to the incidence angle dependency**, the differential phase should be compensated taking into account the slightly different incidence angles of the master and the equivalent monostatic satellites.**
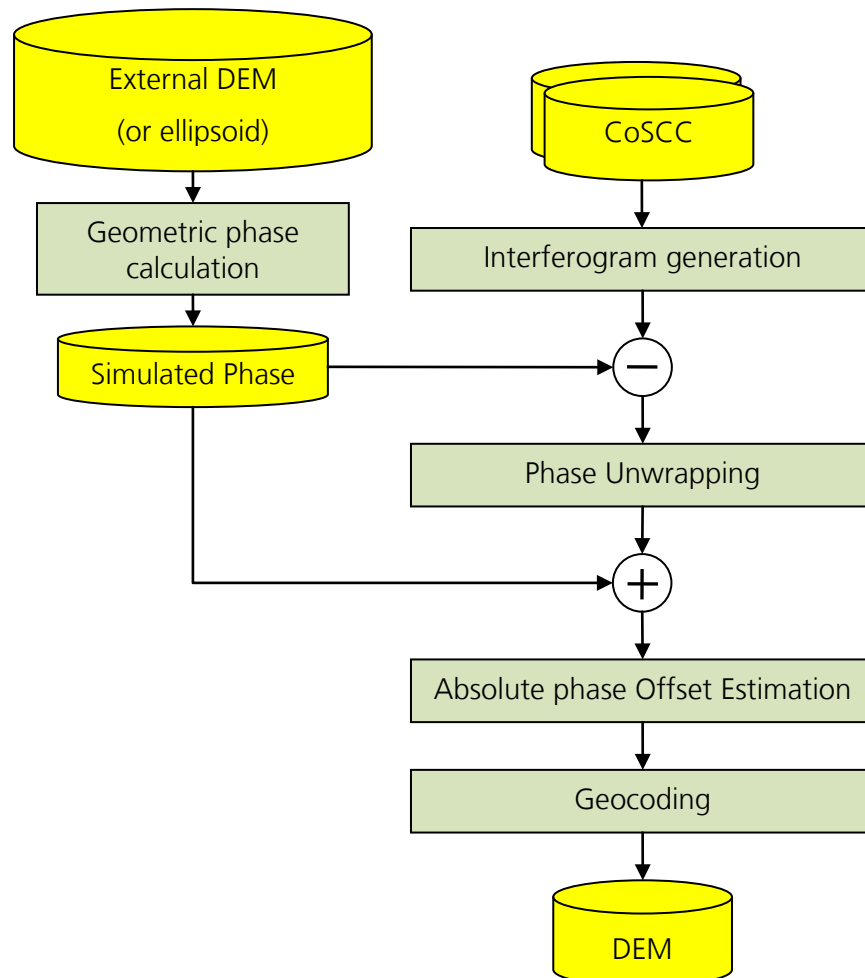

Fig. 17: DEM generation workflow.

Remote Sensing Technology Institute

TanDEM-X Payload Ground Segment
CoSSC Generation and Interferometric Considerations
- Public -

Doc.: **TD-PGS-TN-3129**
Issue: 1.0
Date: 15.05.2012
Page: 23 of 31

5 POLARIZATION CONSIDERATIONS

The operational dual pol combinations for the TerraSAR-X mission that can be currently commanded are

- HH/VV, HH/HV, VV/VH in stripmap mode and

- HH/VV for the spotlight and high resolution spotlight.

Full "quad" polarization using the Dual Receive Antenna (DRA) is available only for specific experimental stripmap acquisitions for TSX. **The DRA has not been used on TanDEM-X in orbit.**

For the TanDEM-X mission, the number of polarization combinations increases considerably. **Only those combinations where the polarizations match are coregistrated based on signal coherent cross correlation**. These combinations are automatically interferometrically processed as operational products by ITP.

One of the TSX/TDX characteristics is the capability to toggle the TX and RX polarization between pulses. This also derives in a larger number of possible polarization combinations. If the commanded sequence matches, the data take is called **Interferometric Dual Pol** (e.g. active satellite 1 HH VV - passive satellite 2 HH VV or active satellite 1 HH HV – passive satellite 2 HH HV). If the commanding does not match the data take is called **Double Pol**. It can be **Double Single Pol** (no toggling) or **Double Dual Pol** (toggling), for example:

- Double Single Pol: HH – HV, VV – VH, HV – HH or VH – VV.

- Double Dual Pol: HH VV – HV VH, HV VH – HH VV, …

Only the interferometric dual pols products are processed by the operational processor. The other products are experimental and they are provided on best effort basis as CoSSC. Notice that for the experimental products where the commanding polarizations do not match, the coregistration is based on a reference DEM. Therefore, the coregsitration may not be accurate.

The use of toggling implies to double the PRF of the system and as consequence **the swath in range is divided by two** (Fritz T. 2012). **The commanding of a Double Dual Pol acquisition can give some additional information about the scattering mechanisms involved in the observed scene**, similar to have a "full pol" acquisition. In this case, it has to be noticed that the receivers are located at different positions. Therefore, **it has to be taken into account the bistatic acquisition geometry and the different paths travelled by the signal when using the phase information**. Again, the satellites' focusing positions, the ZDTs, have to be retrieved in order to properly compensate the phase term due to different paths travelled by the transmitted signal.

Remote Sensing Technology Institute

**TanDEM-X Payload Ground Segment
CoSSC Generation and Interferometric Considerations**
- Public -

Doc.: **TD-PGS-TN-3129**
Issue: 1.0
Date: 15.05.2012
Page: 24 of 31

6 ALTERNATING BISTATIC EXTENSION

6.1 ACQUISITION DESCRIPTION

The alternating bistatic acquisition mode is an operational mode where the transmitter role is switched from pulse to pulse between both satellites. Fig. 8 shows an acquisition scheme of the alternating bistatic mode where the master satellite is highlighted in red for each pulse. Thus**, two bistatic** and **two monostatic** channels are recorded in a **single-pass** of the two satellites. The PRF of each channel is preserved to guarantee a low Azimuth Ambiguity to Signal Ratio (ASSR), around 3KHz (Krieger et al. 2007). Thus, the total PRF of each sensor is doubled and amounts around 6 KHz. Consequently, **the swath width in range is divided by a factor of two** (Krieger et al 2007, Fritz T. 2012).
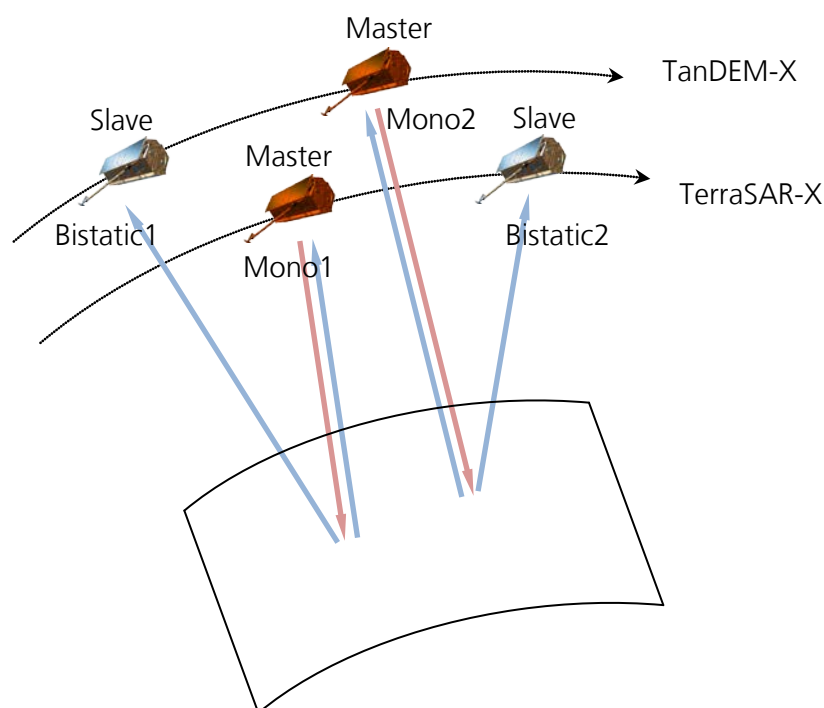

Fig. 18: Alternating bistatic acquisition mode. The transmitter role is switched from pulse to pulse between both satellites. The master satellite is highlighted in red for each pulse. Two bistatic (Bistatic1 and Bistatic2) and two monostatic images (Mono1 and Mono2) are acquired.

The obtained CoSSC products in the alternating bistatic mode are three. Two of them are the result of combining the monostatic and the bistatic channel relative to each master satellite acquisition (Mono1 – Bistatic1 and Mono2 – Bistatic2), bistatic CoSSCs. The third one is due to combine the two monostatic channels (Mono1 – Mono2), monostatic CoSSC. Therefore, **there will be two bistatic CoSSCs and one monostatic**.

The interferometric phase will present **different height sensitivity** between the monostatic and the bistatics CoSSCs. The monostatic CoSSC height of ambiguity is given by

Remote Sensing Technology Institute

TanDEM-X Payload Ground Segment
CoSSC Generation and Interferometric Considerations
- *Public* -

Doc.: **TD-PGS-TN-3129**
Issue: 1.0
Date: 15.05.2012
Page: 25 of 31

(15) $\qquad h_{amb,mono} = \dfrac{\lambda R \sin(\theta_{inc})}{2 \cdot B_n}$,

where R and θ_{inc} are the range and the incidence angle while B_n is the normal baseline respect to the line of sight. However, the height sensitivity for the bistatic CoSSCs is

(16) $\qquad h_{amb,bist} = \dfrac{\lambda R \sin(\theta_{inc})}{B_n}$.

The alternating bistatic mode can be single or dual pol. **The polarization switch in the dual pol mode is linked to the master satellite switch.**

6.2 COREGISTRATION

In the Alternating Bistatic mode, the three CoSSC are generated independently. Therefore, each SSC is only coregistered with its pair located in the same CoSSC container. As a consequence, the acquired channels are not coregistered to a unique master. The coregistration is carried out based on signal if there is enough coherence. If the coherence level is low, as it would be expected on a commanding with different polarizations, the coregistration is made by means of a not reliable fallback solution based on a reference DEM. In this case, **the user may want to perform a coregistration of the images by himself for improving coherence and accuracy**.

If the user desires to have **all the four channels**, the two bistatic and the two monostatic, **referred to one master, the channels need to be cropped and resampled.** As it is not straight forward to coregister all respect to one master, a proposed methodology is given in this subsection. **The first step will be to coregister the two monostatic ones**, Monostatic1 – Monostatic2. This stage does not contain any bistatic particularity, however, some of the intermediate products will be useful to crop and coregister the bistatic channels.

6.2.1 MONOSTATIC 1 – MONOSTATIC 2 COREGISTRATION

The monostatic channel of the first CoSSC will be taken as the master channel, *"Mono1"* in Fig. 18. The rest of the channels will be coregistered to this master channel. **The first step is to coregister the two monostatic images**, *"Mono1"* and *"Mono2"*. Some of the intermediate coregistering products will be useful to coregister the two bistatic images. Fig. 19 shows a proposed workflow to coregister the two monostatic channels. The intermediate products to be used later are highlighted in red. To coregister the two monostatic channels is a well known problem. The workflow showed here is just a proposed one and the user may want to implement his own. **The keypoint is to keep in mind that the intermediate products are necessary for later on coregister the bistatic images.**
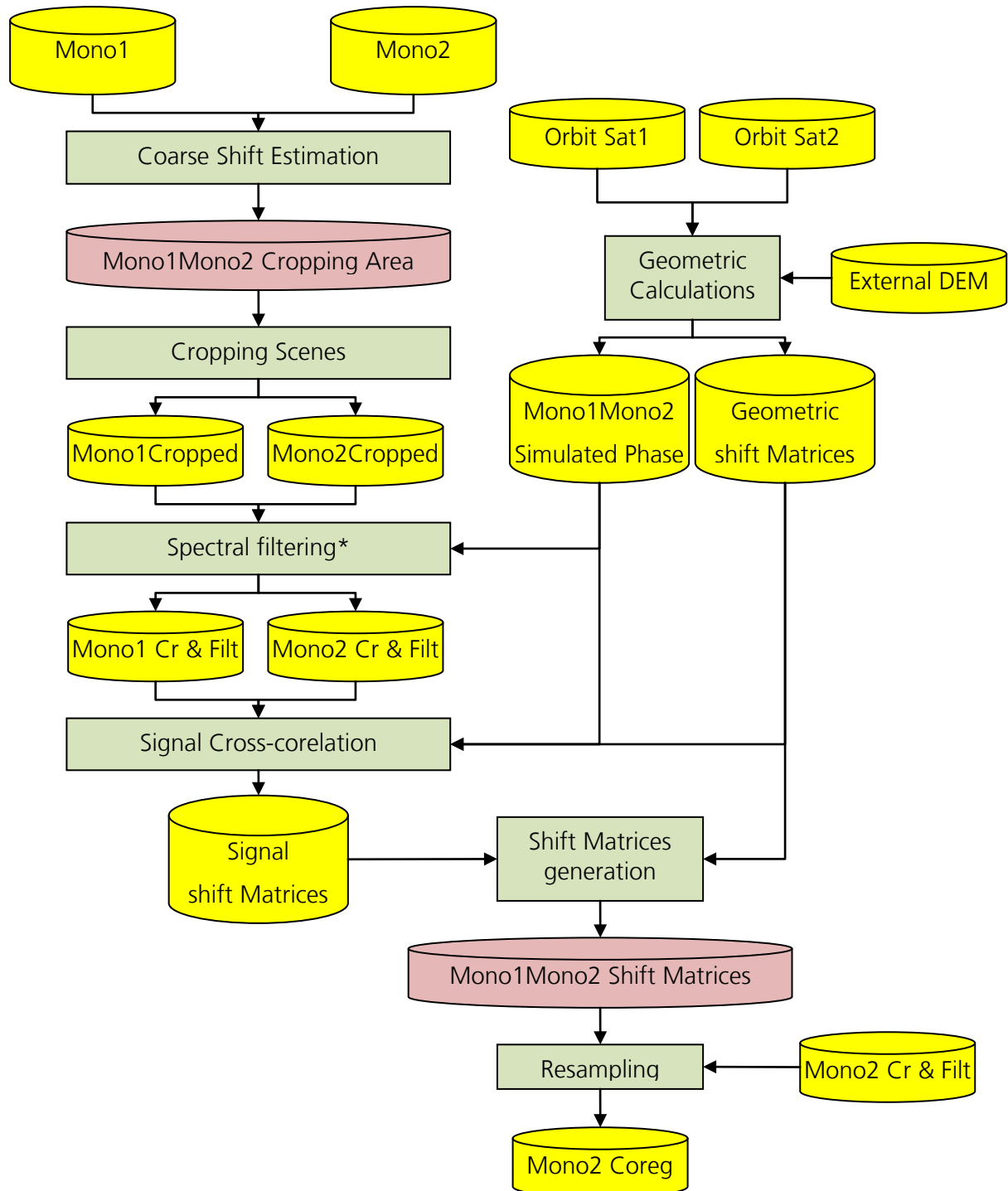
Remote Sensing Technology Institute

TanDEM-X Payload Ground Segment
CoSSC Generation and Interferometric Considerations
- Public -

Doc.: **TD-PGS-TN-3129**
Issue: 1.0
Date: 15.05.2012
Page: 26 of 31

Fig. 19: Proposed workflow to coregister the monostatic acquisitions (Mono1 and Mono2).
*The spectral filtering stage is optional since the images have been already filtered and the shift
between the two spectra is small due to the satellite's close formation.

The main stages of the monostatic coregistration are discussed below as the important middle products:

- *Coarse shift estimation*: A coarse shift estimation should be performed in order to estimate a global shift of the two monostatic channels. **This is needed to crop the SSCs to the common area**. It can be carried out using the coordinates on the ground of the center point

Remote Sensing Technology Institute

TanDEM-X Payload Ground Segment
CoSSC Generation and Interferometric Considerations
- Public -

Doc.: **TD-PGS-TN-3129**
Issue: 1.0
Date: 15.05.2012
Page: 27 of 31

of the scene of the master channel provided on its XML annotation file (*<sceneInfo><sceneCenterCoord><lat/lon>*). Thus, the related range-azimuth integer coordinates for the second monostatic channel should be calculated. They can be obtained taking into account the second monostatic satellite's orbit, the ground coordinates and taking into account the focusing is carried on in ZDT. Therefore, it is possible to establish a global pixel offset for the two channels and the common area. **This is one of the important middle products that will be used later on to coregister the two bistatic channels, it is defined in Fig. 19 as *"Mono1Mono2 Cropping Area"*.**

- *Cropping Scenes*: The two monostatic channels are cropped to the common area according to the obtained *"Mono1Mono2 Cropping Area"*.

- *Spectral filtering*: This step is *optional*, since **the monostatic channels have been already filtered to the common spectra with their respective bistatic pairs**. The relevance of filtering the common spectra depends also on the final application. In practice the spectral displacement of the acquisitions is small due to the short separation between the satellites. However, if it is desired to filter the channels, **it is needed to calculate a simulated phase**. The fringe frequency on the simulated phase will be related to the spectral shift between both acquisitions. This phase can also be used for further interferometric processing stages. It can be calculated taking into account the two acquisitions orbits, the monostatic ZDTs and an external DEM. **The geometrical range/azimuth shift matrices can be also derived from the monostaic geometric calculations.**

- *Signal Cross-corelation*: To coregister the two channels with subpixel accuracy a signal cross-corelation method is suggested. The cross-corelation can be done using different patches arranged on the master monostatic channel grid. If the geometric shift matrices have been calculated before, they can be used to a priori maximize the common area of the patches. **The outputs of this step are the "Signal Shift Matrices".**

- *Shift Matrices Generation*: The final shift matrices have to be generated. The Signal Shift Matrices can also contain a quality estimation of the obtained shift. This estimation is based on how good the correlation between the two signals is. If the geometric shift matrices have been calculated, they can substitute the *"Signal Shift Matrices"* where they present a low correlation level. **The output of this stage are the *"Mono1-Mono2 shift Matrices"*. This is an important result to be used for the coregistration of the bistatic channels.**

- *Resampling*: Once the channels are cropped and the shift matrices have been generated, it is possible to properly resample the second monostatic channel to match the master one with a subpixel accuracy.

6.2.2 MONOSTATIC 1 – BISTATIC 2 COREGISTRATION

The proposed workflow to coregister the second bistatic channel is illustrated in Fig. 20. The main stages are practically the same as in the previous monostatic coregistration. **Notice that in this case, the Cropping Area and the Shift Matrices calculated in the monostatic1-monostatic2 coregistration are used as input**. If it is desired to carry out the spectral filter or if it is needed to perform further interferometric processes, the bistatic simulated phase should be computed. **In order to calculate the bistatic interferometric phase, the bistatic ZDTs should be obtained as explained in Section 3.**
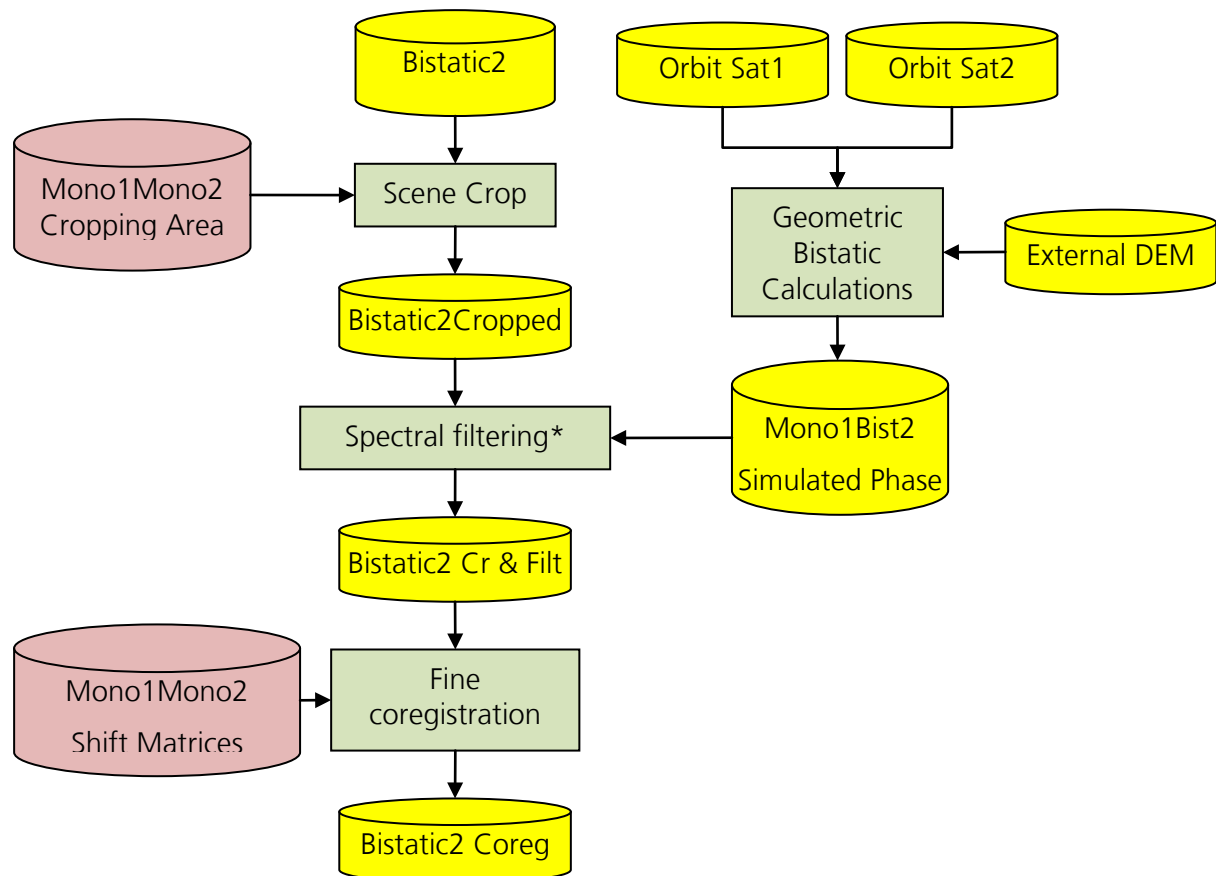
Remote Sensing Technology Institute

TanDEM-X Payload Ground Segment
CoSSC Generation and Interferometric Considerations
- Public -

Doc.: **TD-PGS-TN-3129**
Issue: 1.0
Date: 15.05.2012
Page: 28 of 31

Fig. 20: Workflow to coregister the master image, Mono1, to the second bistatic acquisition, Bistatic2. The inputs obtained in the Mono1-Mono2 coregistration are highlighted in red. *The spectral filtering stage is optional since the images have been already filtered and the shift between the two spectra is small due to the satellite's close formation.

6.2.3 MONOSTATIC 1 – BISTATIC 1 COREGISTRATION

Finally, in order to match all the channels with respect one master (the first monostatic image, Mono1), the first bistatic channel (Bistatic1) should be cropped. In this way, all the channels will refer to the same common area (Fig. 21 left). **Notice that in this case it is not needed to filter neither to resample the bistatic channel since it has been already filtered and resampled during the CoSSC formation.** If it is desired to carry out further interferometric processing, the bistatic simulated phase should be computed taking into account the bistatic geometry and, again, deriving the bistatic ZDTs as described in Section 3 (Fig. 21 right).

Remote Sensing Technology Institute
TanDEM-X Payload Ground Segment
CoSSC Generation and Interferometric Considerations
- Public -

Doc.: **TD-PGS-TN-3129**
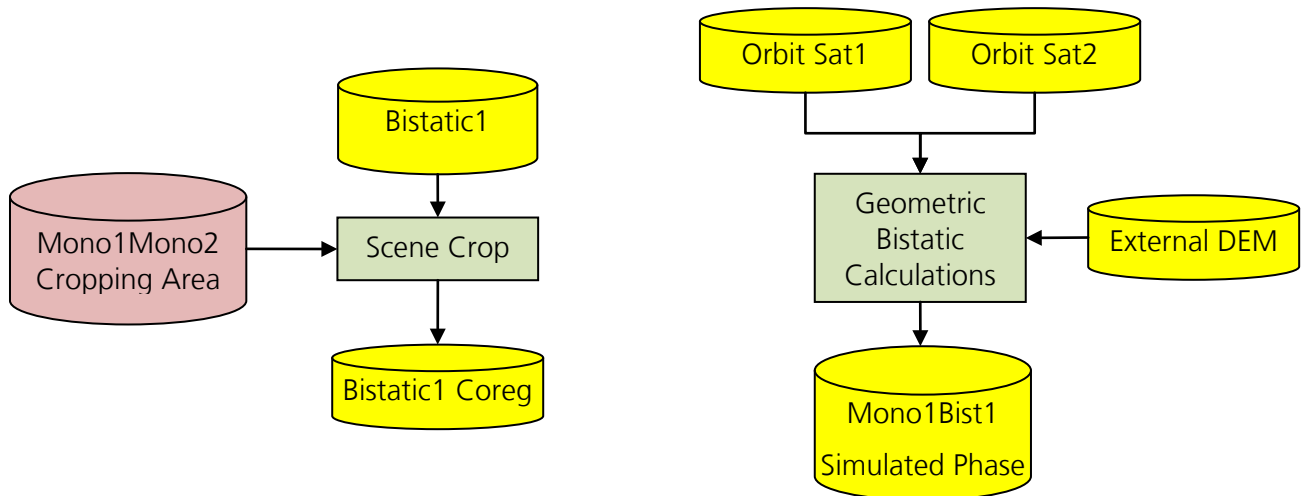Issue: 1.0
Date: 15.05.2012
Page: 29 of 31

Fig. 21: Workflow to crop the first bistatic image to the common area of the alternating bistatic acquisitions (left). Workflow to obtain the bistatic simulated interferometric phase for Mono1 – Bistatic1.

6.3 POSSIBLE ALTERNATING BISTATIC APPLICATIONS AND UTILITIES

The novel alternating bistatic acquisition mode arises a new field of possible applications and utilities. This mode can be used **internally to improve the synchronization between both satellites and reduce the impact of oscillator discrepancies**, providing a more stable interferometric bistatic phase (Krieger & Younis 2006). Besides, for the users, it can be useful for the demonstration of **new applications taking advantages of acquiring a monostatic and bistatic interferogram at the same time**. Some of the future possible applications and utilities of this mode are listed below:

- *Phase unwrapping improvement*. As said on the previous subsection, the availability of two interferograms with different height sensibilities can be helpful to **resolve phase unwrapping ambiguities**.

- *Scattering mechanism study*. The monostatic and bistatic interferograms acquired in a single-pass **provide additional information to retrieve some characteristics of volumetric scattering** (Treuhaft & Siquiera 2000) and it would also be possible to **distinguish between direct and double-bounce scattering from the ground** (Ballester-Berman & Lopez-Sanchez 2007). Also, as said on the previous section, **the use of different polarizations in the commanding can give some information about the scattering mechanisms involved in the observed scene.** For this, the bistatic geometry and the phase term due to the different paths travelled by the signal have to be taken into account.

  In this case, it has to be noticed that the receivers are located at different positions. Therefore, it has to be taken into account the bistatic acquisition geometry and the different paths travelled by the signal for using the phase information.

- *Statistic measurements*. **The two bistatic pairs can be also considered as a two image realizations of the observed scene**. Therefore, some statistical computation can be done using both images instead of just one. For example, in the case of the coherence estimation, the looks can take into account samples in the two bistatic interferograms, which would result in a lower spatial resolution loss.

Remote Sensing Technology Institute

TanDEM-X Payload Ground Segment
CoSSC Generation and Interferometric Considerations
- Public -

Doc.: **TD-PGS-TN-3129**
Issue: 1.0
Date: 15.05.2012
Page: 30 of 31

7 BIBLIOGRAPHY

Ballester-Berman, J., & Lopez-Sanchez, J. (2007). Coherence loci for a homogeneous volume over a double bounce ground model. *IEEE Geoscience and Remote Sensing Letters*, Vol 4, No 2, pages 317 - 321.

Balss, U., Niedermeier, A., & Breit, H. (2010). TanDEM-X Bistatic SAR Processing. *EUSAR.* Aachen.

Bamler, R., Meyer, F., & Liebhart, W. (November 2007). Processing of Bistatic SAR Data From Quasy-Stationary Configurations. *IEEE TRANSACTIONS ON GEOSCIENCE AND REMOTE SENSING*, Vol 45, No 11, pages 3350 - 3358.

Breit, H., Fritz, T., Balss, U., Niedermeier, A., & Vonavka, M. (February 2010). TerraSAR-X SAR Processing and Products. *IEEE TRANSACTIONS ON GEOSCIENCE AND REMOTE SENSING*, Vol 48, No 2, pages 727 - 740.

Constantini, M. (1998). A novel phase unwrapping method based on network programming. *IEEE TRANSACTIONS ON GEOSCIENCE AND REMOTE SENSING*, Vol 36, No 3, pages 813 - 821.

Curlander, J., & McDonough, R. (1991). Geometric calibration of SAR data. In J. C. Curlander, & R. N. McDonough, *Synthetic Aperture Radar. Systems and Signal Processing.* John Willey & Sons, Inc.

Eineder, M., & Adam, N. (2005). A maximum-likelihood estimator to simultaneously unwrap, geocode, and fuse SAR interferograms from different viewing geometries into one digital elevation model. *IEEE TRANSACTIONS ON GEOSCIENCE AND REMOTE SENSING*, Vol 43, No 1, pages 24-36.

Eineder, M., Hubig, M., & Milcke, B. (1998). Unwrapping large interferograms using the minimum cost flowalgorithm. *IGARSS.* Seattle.

Fritz, T. (2012). *TanDEM-X Experimental Product Description.* TD-GS-PS-3028.

Fritz, T., Rossi, C., Yague-Martinez, N., Rodriguez-Gonzalez, F., Lachaise, M., & Breit, H. (2011). Interferometric processing of TanDEM-X daa. *IGARSS*, (pp. 2428 - 2431). Vancouver.

Gläßer, H., Schwinger, M., Seifert, P., Fritz, T., & Balzer, W. (2010). TanDEM-X Data Driven Workflow in Payload Ground Segment. *EUSAR.* Aachen.

Krieger, G., & Younis, M. (2006). Impact of Oscillator Noise in Bistatic and Multistatic SAR. *IEEE Geoscience and Remote Sensing Letters*.

Krieger, G., Moreira, A., Fiedler, H., Hajnsek, I., Werner, M., Younis, M., et al. (2007). TanDEM-X: A Satellite Formation for High-Resolution SAR Interferometry. *IEEE TRANSACTIONS ON GEOSCIENCE AND REMOTE SENSING*, Vol 45, No 11, pages 3317 - 3341.

M. Jehle, M., Perler, D., Small, D., Schubert, A., & Meie, E. (2008). Estimation of atmospheric path delays in TerraSAR-X data using models vs. measurements. *Sensors*, Vol 8, No 12, pages 8479-8491.

Rossi, C., Rodriguez-Gonzalez, F., Fritz, T., Yague Martinez, N., & Eineder, M. (2012). TanDEM-X Calibrated Raw DEM Generation. *International Society for Photogrammetry and Remote Sensing (ISPRS)*, submitted.

Rossi, D., Eineder, M., Fritz, T., & Breit, H. (2010). TanDEM-X Mission: Raw DEM Generation. *EUSAR.* Aachen.

Remote Sensing Technology Institute

TanDEM-X Payload Ground Segment
CoSSC Generation and Interferometric Considerations
- Public -

Doc.: **TD-PGS-TN-3129**
Issue: 1.0
Date: 15.05.2012
Page: 31 of 31

Sansosti, E., Berardino, P., Manunta, M., Serafino, F., & Fornaro, G. (October 2006). Geometrical SAR Image Registration. *IEEE TRANSACTIONS ON GEOSCIENCE AND REMOTE SENSING*, Vol 44, No 10, pages 2861 - 2870.

Treuhaft, R., & Siquiera, P. (2000). The vertical structure of vegetated land surfaces from interferometric and polarimetric radar. *Radio Science*, Vol 35, No 1, pages 141 - 177.

Wegmüller, U. (1999). Automated terrain corrected SAR geocoding. *IGARSS.* Hamburg.

Yague-Martinez, N., Eineder, M., Brcic, R., Breit, H., & Fritz, T. (2010). TanDEM-X Mission: SAR Image Coregistration Aspects. *EUSAR.* Aachen.